

# Relationship between tropical cloud feedback and climatological bias in clouds

Chad W. Thackeray,<sup>1\*</sup> Mark D. Zelinka,<sup>2</sup> Jesse Norris,<sup>1</sup> Alex Hall,<sup>1</sup> Stephen Po-Chedley<sup>2</sup>

<sup>1</sup> Department of Atmospheric and Oceanic Sciences, University of California, Los Angeles, Los Angeles, California.

<sup>2</sup> Atmospheric, Earth, and Energy Division, Lawrence Livermore National Laboratory, Livermore, California.

\*[cwthackeray@ucla.edu](mailto:cwthackeray@ucla.edu)

## Key Points:

- We find a relationship between tropical cloud feedback and mean-state biases in Southern Hemisphere extratropical cloud properties.
- This intermodel relationship is found to be present in three different ensembles of global climate models, a sign of robustness.
- This relationship suggests a likely tropical cloud feedback value of  $0.52 \pm 0.34$  W/m<sup>2</sup>/K, which equates to a 34% reduction in uncertainty.

## 1 **Abstract**

2 Global climate model (GCM) projections of future climate are uncertain largely due to a  
3 persistent spread in cloud feedback. This is despite efforts to reduce this model uncertainty  
4 through a variety of emergent constraints (ECs); with several studies suggesting an important role  
5 for present-day biases in clouds. Here, we use three generations of GCMs to assess the value of  
6 climatological cloud metrics for constraining uncertainty in cloud feedback. We find that  
7 shortwave cloud radiative properties across the Southern Hemisphere extratropics are most  
8 robustly correlated with tropical cloud feedback (TCF). Using this relationship in conjunction  
9 with observations, we produce an EC that yields a TCF value of  $0.52 \pm 0.34 \text{ W/m}^2/\text{K}$ , which  
10 equates to a 34% reduction in uncertainty. Thus, we show that climatological cloud properties can  
11 be used to reduce uncertainty in how clouds will respond to future warming.

## 12 **Plain Language Summary**

13 Different global climate models exhibit large variability in how clouds across the tropics will  
14 respond to future warming. This is largely due to the complexity and diversity of responses that  
15 differing cloud types may experience under warming. A long-term goal of the community has  
16 been to narrow this disagreement between different models. Over the past 15 years, several  
17 studies have proposed ways in which the variability in future cloud changes might be related to  
18 errors in how these models represent present-day properties. Here, we use three collections of  
19 models to show that variability in tropical cloud changes is closely tied to shortwave cloud  
20 radiative properties across the Southern Ocean. We then use this intermodel relationship along  
21 with observations to produce a best estimate of cloud feedback across the tropics.

## 22 **1. Introduction**

23 Global climate models (GCMs) have long disagreed about how clouds will respond to future  
24 warming, as exemplified by a large and persistent intermodel spread in cloud feedback (Cess et al.  
25 1990; Bony and Dufresne, 2005; Bony et al. 2006; Webb et al. 2013; Zelinka et al. 2020). Given  
26 that cloud feedback is the largest source of uncertainty for model estimates of equilibrium climate  
27 sensitivity (ECS) (Caldwell et al. 2016; Sherwood et al. 2020), there has been a major emphasis  
28 on determining which projected cloud changes are most likely. Emergent constraints (ECs) are a  
29 popular approach to tackling this problem as they use intermodel relationships between current  
30 and future climate metrics in conjunction with observations to narrow uncertainty (Klein and Hall  
31 2015; Williamson et al. 2021). Past studies have suggested that both observable cloud variations  
32 with temperature change (Qu et al. 2014; Zhai et al. 2015; Zhou et al. 2015; Brient and Schneider  
33 2016; Jiang et al. 2023) and climatological biases in cloud or radiative properties (Williams and  
34 Tselioudis 2007; Volodin 2008; Trenberth and Fasullo 2010; Klein et al. 2013; Brient et al. 2016;  
35 Lipat et al. 2017; Siler et al. 2018) might directly affect cloud feedback, and thus ECS.

36 Here we focus on the latter hypothesis, and briefly discuss two proposed mean-state biases  
37 of relevance to global cloud feedback (GCF). Building off Volodin (2008), Siler et al. (2018) use  
38 the Fifth Coupled Model Intercomparison Project (CMIP5) to find a strong relationship between  
39 GCF/ECS and the difference in cloud contributions to albedo between regions of warm versus  
40 cool (separated by 23.5°C isotherm) sea surface temperatures (SSTs) (derived as a projection of  
41 each model's albedo climatology onto the albedo-GCF correlation map). They also show that the  
42 contrast in top-of-atmosphere (TOA) shortwave cloud radiative effect (SWCRE) between these  
43 two regions is a strong predictor of GCF. This study indicates that the present-day distribution of  
44 clouds could inform future cloud changes through cloud albedo's dependence on SSTs and the  
45 future expansion of warm SSTs. However, the physical reasoning behind the constraint has been  
46 questioned (Caldwell et al. 2018).

47 Another example suggests that the present-day TOA energy balance across the Southern  
48 Hemisphere (SH) is strongly tied to ECS in CMIP3 (Trenberth and Fasullo 2010). They argue that  
49 GCMs with less cloud cover (and thus a more positive TOA radiative imbalance) across the  
50 Southern Ocean might have greater potential for increased cloud cover in a warming climate.  
51 However, this relationship was negligible in CMIP5 (Grise et al., 2015). Moreover, the CMIP3  
52 relationship was found to be driven by a subset of GCMs characterized by unrealistically bright  
53 present-day clouds in the SH subtropics. Instead, Grise et al. (2015) pointed to present-day cloud  
54 and net radiation biases in subtropical stratocumulus-to-cumulus transition regions as important  
55 for explaining ECS variability.

56 This exemplifies a common issue encountered with proposed constraints on ECS and  
57 GCF: failed “out-of-sample” testing (Caldwell et al. 2018; Schlund et al. 2020), where a proposed  
58 relationship is not found in a different ensemble (Hall et al. 2019). Given these difficulties,  
59 several recent efforts have targeted specific cloud regimes (Qu et al. 2015; Terai et al. 2016;  
60 Myers and Norris, 2016; McCoy et al. 2020; Myers et al. 2021; Hirota et al. 2021) or regions  
61 (Lutsko et al. 2021; Wall et al. 2022) with the prevailing thought being that it is unlikely for a  
62 single current climate metric to robustly explain uncertainty in the highly complex ECS or GCF  
63 (Sherwood et al. 2020).

64 Here, we use three generations of GCMs to assess the potential value of climatological  
65 cloud biases for constraining regional cloud feedbacks. We primarily focus on metrics that have  
66 been shown to strongly correlate with either ECS or GCF in prior studies as these relationships  
67 likely exploit some regional relationship, which happens to control intermodel spread.

## 68 **2. Data and Methods**

### 69 **2.1 Climate Models**

70 We use output from a collection of 55 GCMs from the three most recent phases of CMIP  
71 (CMIP3, CMIP5, CMIP6) (Meehl et al. 2007; Taylor et al. 2012; Eyring et al. 2016) (Tables S1-

72 3). Model data comes from the first realization of the pre-industrial control (piControl), AMIP,  
73 and abrupt-4xCO<sub>2</sub> experiments. The latter is a 150-year simulation in which the atmospheric CO<sub>2</sub>  
74 is instantaneously quadrupled from pre-industrial levels and then held fixed. The abrupt forcing  
75 experiment was not run for CMIP3, so we rely on the 1pctCO<sub>2</sub> experiment instead. We use ECS  
76 values from Zelinka et al. (2020) for CMIP5/6 and model development papers for CMIP3.

## 77 **2.2 Cloud Metrics**

78 Cloud feedback is calculated following Zelinka et al. (2020) for CMIP5 and CMIP6 models. First,  
79 annual anomalies are computed using the abrupt-4xCO<sub>2</sub> experiment with respect to  
80 contemporaneous 21-year running means from piControl to account for possible model drift  
81 (Caldwell et al. 2016). Cloud feedback is then derived by adjusting the TOA CRE (clear-sky  
82 minus all-sky upwelling flux) feedback for non-cloud effects (Soden et al. 2008; Shell et al.,  
83 2008). For CMIP3, we calculate the SWCRE feedback by first computing anomalies of SWCRE  
84 averaged over years 60-80 from the 1pctCO<sub>2</sub> experiment (surrounding the point when  
85 atmospheric CO<sub>2</sub> has doubled) relative to the same years of piControl. These anomalies are then  
86 normalized by the change in global and annual mean surface air temperature. Because these  
87 CMIP3 results are not directly comparable to those of CMIP5/6, we only consider the latter when  
88 building an EC on cloud feedback.

89 We also calculate several climatological cloud metrics. All climatological metrics used  
90 throughout are calculated as 30-year means derived from each piControl simulation (years 100-  
91 130 or the last 30 years if less than 130 years are available) and remapped to a common 2.5°x2.0°  
92 grid. (Note that for AMIP results, we use the entire simulation period for each ensemble.) The  
93 metrics evaluated here include SW and LW CRE at both the surface (SFC) and TOA, total cloud  
94 cover (CLT), and condensed water path (CWP). TOA CRE is defined as the clear- minus all-sky  
95 upwelling radiative flux at the TOA. CRE at the SFC is defined by subtracting the all- minus  
96 clear-sky surface upwelling flux from the all- minus clear-sky surface downwelling flux. We will

97 primarily focus on SFC SWCRE rather than TOA because it exhibits a slightly better correlation  
98 with cloud feedback, but these terms are strongly correlated across models ( $r=0.96$ ). We assess  
99 CLT because many GCMs do not provide the appropriate variables for cloud fraction at differing  
100 levels of the atmosphere.

101 Lastly, we break down simulated SWCRE into contributions from cloud albedo and cloud  
102 amount to interpret model biases. TOA SWCRE can be derived from the clear- and all-sky SW  
103 radiative fluxes:

$$104 \quad \text{SWCRE} = \text{SW}_{\text{clr}} - \text{SW}_{\text{all}} = \text{CLT} * (\text{SW}_{\text{clr}} - \text{SW}_{\text{ov}}) \quad (1)$$

105 where  $\text{SW}_{\text{ov}}$  is the overcast SW radiative flux, which can be computed from (2).

$$106 \quad \text{SW}_{\text{all}} = \text{CLT} * \text{SW}_{\text{ov}} + (1-\text{CLT}) * \text{SW}_{\text{clr}} \quad (2)$$

107 The difference in SWCRE either between two groups or with respect to a given GCM's ensemble  
108 mean can then be decomposed into two components:

$$109 \quad \Delta\text{SWCRE} = \Delta\text{CLT} * (\text{SW}_{\text{clr}} - \text{SW}_{\text{ov}}) + \text{CLT} * \Delta(\text{SW}_{\text{clr}} - \text{SW}_{\text{ov}}) \quad (3)$$

110 The first term (cloud amount contribution) is derived by holding the radiation contrast term  
111 (essentially cloud albedo) constant, while the second term is derived from holding the cloud  
112 fraction constant.

### 113 **2.3 Observational Data**

114 An observational estimate of climatological SFC SWCRE is computed from the Clouds and the  
115 Earth's Radiant Energy System (CERES) dataset (Kato et al. 2018). Since surface products from  
116 CERES are more uncertain than their TOA counterparts (Loeb et al. 2018), we also calculate SFC  
117 SWCRE from ECMWF Reanalysis version 5 (ERA5; Hersbach et al. 2020, 2023). We use data  
118 from 2001-2021 to derive these climatological means. The average of these two estimates is used  
119 throughout. Since the datasets exhibit such good agreement in extratropical SFC SWCRE, we also  
120 calculate annual average SFC SWCRE to quantify interannual variability in this metric. The

121 standard deviation (or the more conservative range) of these annual values is treated as  
122 observational uncertainty.

## 123 **2.4 Constraint Methods**

124 Constrained estimates of cloud feedback are computed using the hierarchical EC framework of  
125 Bowman et al. (2018). This method accounts for the correlation strength, observational  
126 uncertainty, and the signal-to-noise ratio between observational and GCM uncertainty. The  
127 constrained 95% prediction interval is compared to the unconstrained 95% prediction interval to  
128 measure an EC's value at reducing uncertainty. We also use the EC correlation decomposition  
129 method of Caldwell et al. (2018) to better understand the geographical breakdown of the  
130 relationship between SH extratropical SFC SWCRE and GCF. We adapt their equation 6 as  
131 follows:

$$132 \quad \text{corr}(X, \text{GCF}) = \sigma(\text{CF}_{\text{local}})/\sigma(\text{GCF}) * \text{corr}(X, \text{CF}_{\text{local}}) \quad (4)$$

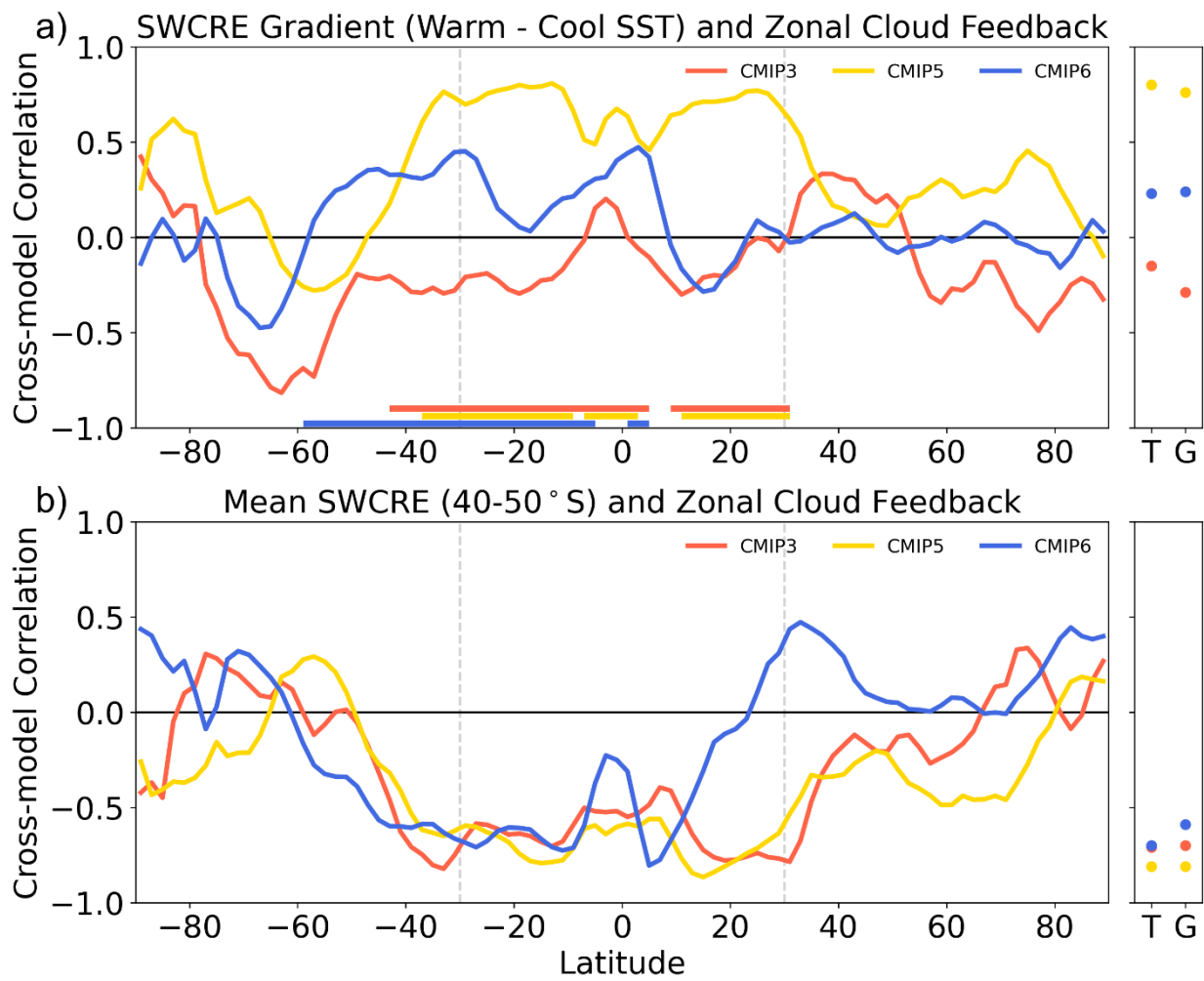
133 The decomposition value at each grid cell is the product of the cross-model correlation  
134 between a current climate metric (denoted by X) and the local cloud feedback ( $\text{CF}_{\text{local}}$ ) (Fig. S1a-  
135 c), and the ratio of  $\text{CF}_{\text{local}}$  variability ( $\sigma$ ; sampled across the ensemble) to GCF variability (Fig.  
136 S1d-f).

## 137 **3. Results**

### 138 **3.1 Relevance of Climatological SFC SWCRE to Cloud Feedback**

139 We first assess how the gradient in climatological SFC SWCRE between warm and cool SST  
140 regions (inspired by Siler et al. 2018) correlates with zonal-mean cloud feedback across three  
141 CMIP generations (Fig. 1a). It is important to gauge EC robustness using multiple ensembles  
142 because a relationship can appear in a single ensemble by chance (Caldwell et al. 2014) and large  
143 changes can occur from one ensemble to the next (Schlund et al. 2020; Text S1; Fig. S2). Strong  
144 correlations are evident over 40°S-30°N for CMIP5, which is expected since this EC was  
145 developed on CMIP5. These latitudes also happen to coincide with regions where zonal-mean

146 cloud feedback is strongly correlated ( $r > 0.7$ ) with GCF (illustrated by bars along the x-axis of Fig.  
 147 1a). Because of this, the gradient metric is strongly correlated with both the tropical cloud  
 148 feedback (TCF; defined as  $30^{\circ}\text{S}$ - $30^{\circ}\text{N}$ ;  $r = 0.80$ ) and GCF ( $r = 0.76$ ). However, we find substantially  
 149 weaker correlations in both CMIP3 ( $r = -0.15$  for TCF,  $-0.29$  for GCF) and CMIP6 ( $r = 0.23$  for  
 150 TCF,  $0.24$  for GCF). Cross-model correlation maps show that this weakening is tied to a less  
 151 positive, or even negative, correlation between SWCRE across warm SST areas and TCF in  
 152 CMIP3 and CMIP6 (Fig. 2a-c). Moreover, in CMIP6, there is a southward shift in which latitudes  
 153 are driving variability in GCF, whereby  $40$ - $60^{\circ}\text{S}$  plays a more important role (Fig. 1a). These  
 154 latitudes are also more important for ECS variability in CMIP6 (Lutsko et al. 2021).



155  
 156 **Fig. 1.** Cross-model correlation between zonal-mean cloud feedback and (a) the gradient in SFC SWCRE between  
 157 areas of warm and cool SSTs inspired by Siler et al (2018), (b) the mean SFC SWCRE over  $40$ - $50^{\circ}\text{S}$ . Individual  
 158 colored lines represent the results for each of the CMIPs. Latitudes where zonal-mean cloud feedback is strongly

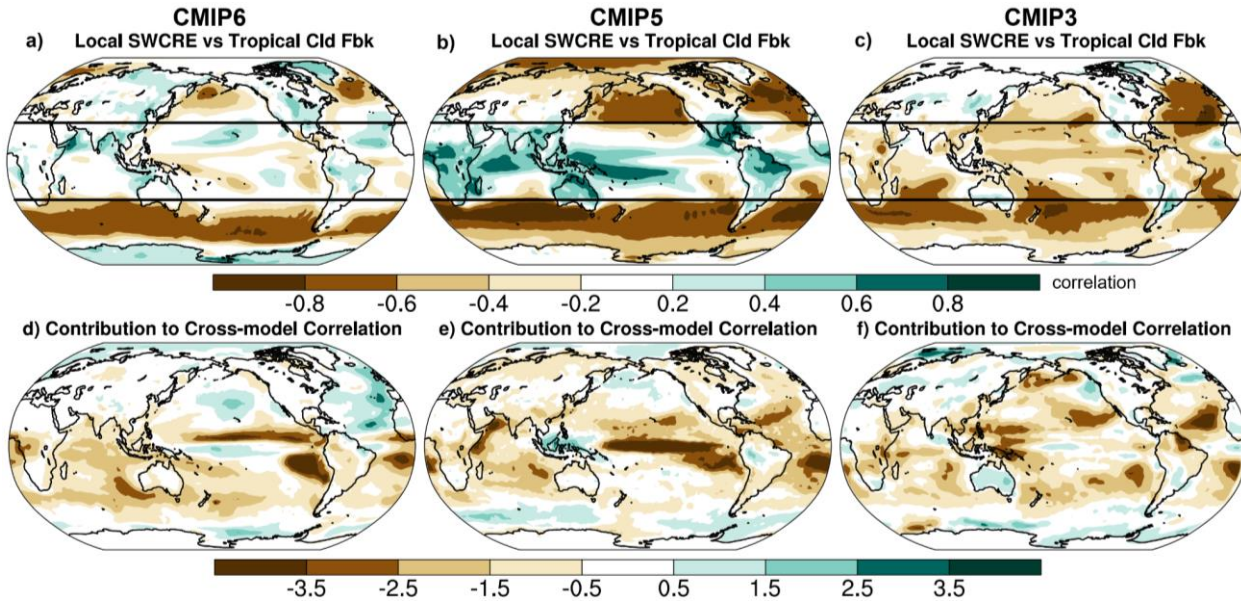


159 correlated ( $r > 0.7$ ) with GCF are illustrated on panel a by horizontal bars along the x-axis. Cross-model correlations  
160 between these metrics and TCF/GCF are also shown on the right panel of each plot as colored dots.

161 Building off prior work which suggests potential connections between SH radiative fluxes  
162 to GCF and ECS (Trenberth and Fasullo 2010; Grise et al. 2015), we also evaluate the relevance  
163 of SWCRE across the SH to zonal-mean cloud feedback. We find that 40-50°S SFC SWCRE is  
164 strongly tied to cloud feedback across much of the 40°S-20°N range in all three ensembles (Fig.  
165 1b). This manifests as a strong negative correlation with TCF, with correlations ranging from -  
166 0.70 in CMIP6 to -0.81 in CMIP5. Because these latitudes tend to control a substantial portion of  
167 intermodel variability in GCF, there is also a strong correlation with GCF in CMIP3 ( $r = -0.70$ ) and  
168 CMIP5 ( $r = -0.81$ ). The CMIP6 result is slightly weaker ( $r = -0.59$ ) given a greater role for the SH  
169 mid-latitudes in controlling GCF and less negative correlations at the equator and north of 15°N.  
170 Weaker equatorial correlations stem from two anomalous GCMs, while the decline polewards of  
171 15°N is driven by weak feedbacks in the CESM2 models (Fig. S3). (Note that similar analysis  
172 was performed for a variety of other metrics (LWCRE, TOA SWCRE, CLT, CWP, and TOA  
173 albedo; Fig. S4) and latitude bands (Fig. S5), but this is not discussed for brevity).

174 Given the robustness of the 40-50°S SFC SWCRE relationships, this will be our focus  
175 going forward. Cross-model correlation maps emphasize that a strong anti-correlation between  
176 TCF and SFC SWCRE over mid-latitude ocean basins is the main persistent feature of this  
177 relationship across generations (Fig. 2a-c). This relationship is particularly robust in the SH,  
178 where climatological cloud cover is very large (Grise et al. 2015; Kay et al. 2016). We can better  
179 understand the relationship between 40-50°S SFC SWCRE and GCF using the correlation  
180 decomposition framework of Caldwell et al. (2018). This method dissects cross-model  
181 correlations to quantify the contribution of a specific region (see Methods). It considers both the  
182 cross-model correlation between 40-50°S SFC SWCRE and the local cloud feedback (Fig. S1a-c),  
183 and the ratio of local cloud feedback variability to GCF variability (Fig. S1d-f). The  
184 decomposition shows large-scale consistency across model generations: larger climatological 40-

185 50°S SWCRE corresponds to greater local cloud feedback throughout the tropics (Fig. 2d-f).  
 186 Regions with important low cloud feedback off the west coasts of South America, Africa, and  
 187 Australia contribute to the negative correlation, but the magnitude and precise locations vary by  
 188 ensemble.

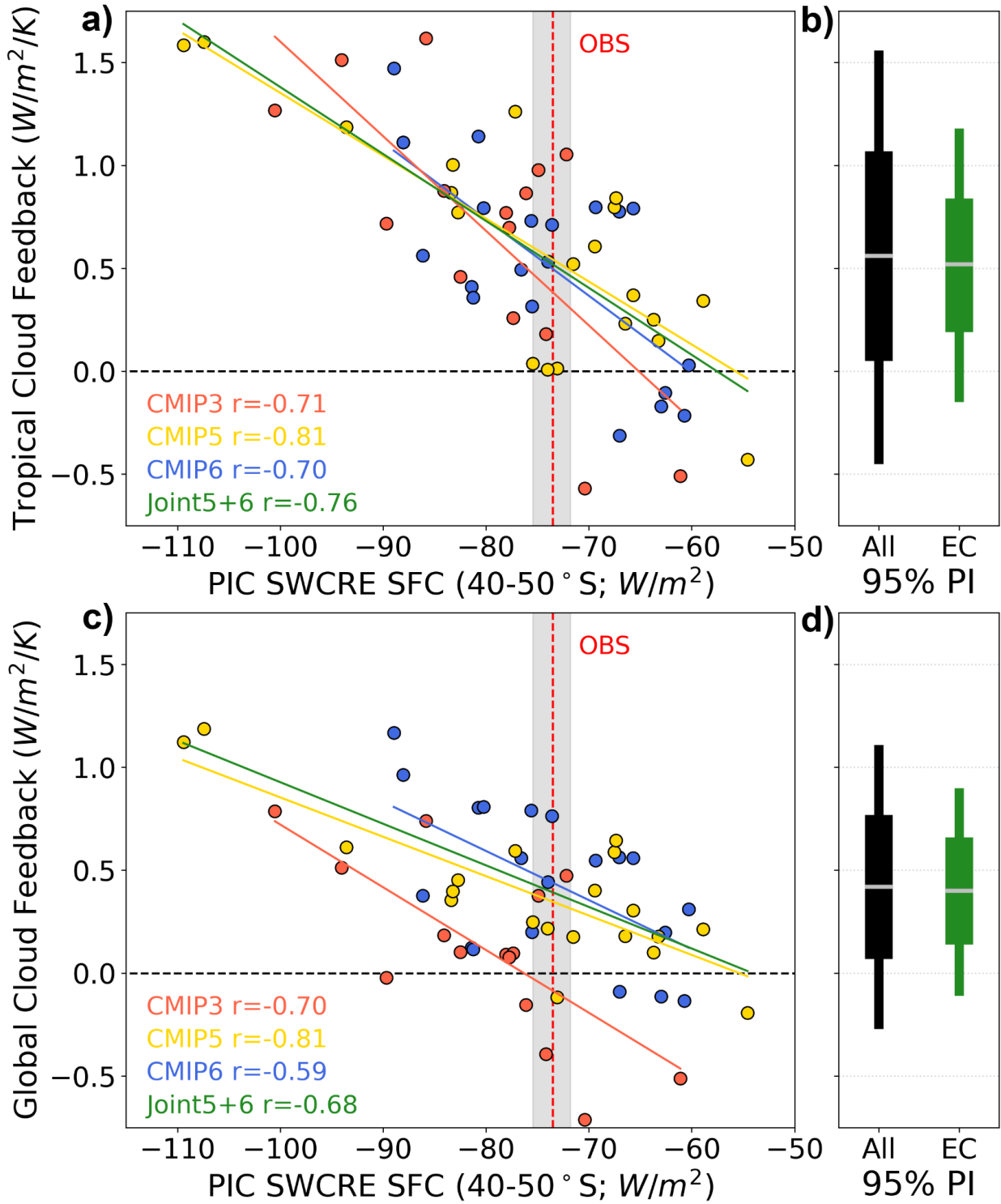


189  
 190 **Fig. 2.** Cross-model correlation maps between local SFC SWCRE and TCF for (a) CMIP6 (b) CMIP5 (c) CMIP3.  
 191 Regionally decomposed cross-model correlation (see Methods) for the relationship between 40-50°S SFC SWCRE  
 192 and GCF following Caldwell et al. (2018) for (d) CMIP6 (e) CMIP5 (f) CMIP3. The local contribution values can be  
 193 spatially averaged to obtain the correlation shown in Figure 2b. Solid black lines denote the tropical region (30°S-  
 194 30°N).

### 195 **3.2 Emergent Constraint on Tropical Cloud Feedback**

196 Given the robustness of this relationship, we build an EC on TCF. In Figure 3a we scatter  
 197 climatological SFC SWCRE averaged across 40-50°S against the TCF. (Note that these  
 198 climatological values are very similar in magnitude and strongly correlated with those derived  
 199 from historical and AMIP simulations). For reference, we also show the relationship with GCF  
 200 (Fig. 3c). Observations from CERES and ERA5 over 2001-2021 are used in conjunction with this  
 201 relationship to form the EC. We derive an estimate of observational uncertainty from interannual  
 202 variability. The observed estimate ( $-73.5 \pm 0.8 \text{ W/m}^2$ ; [66% confidence interval]) suggests that  
 203 GCMs tend to be negatively biased when it comes to SH mid-latitude SFC SWCRE (average of

204 all GCMs:  $-76.1 \pm 11.6 \text{ W/m}^2$ ). CMIP3 is the most consistently negatively biased ( $-79.9 \pm 9.9$   
 205  $\text{W/m}^2$ ), signaling that some progress has been made. However, because the CMIP3 cloud  
 206 feedback values are not derived in the same way as for CMIP5/6 (see Methods), we exclude this  
 207 data when building the EC. Given the similar slopes for each ensemble, we only report results for  
 208 a combined ensemble of CMIP5 and CMIP6 (individual ensemble results are in Text S2).



210 **Fig. 3.** Scatterplot of climatological SFC SWCRE averaged over 40-50°S versus (a) TCF, (c) GCF where each point  
211 represents a different GCM. The vertical dashed red line represents an observed estimate from observations (CERES,  
212 ERA5) while grey shading denotes the range in annual mean values, which is used in the derivation of the EC (see  
213 Methods). (b) 95% prediction interval of TCF for the unconstrained CMIP5/6 ensemble (black) and the EC (green).  
214 (d) same as b but for the GCF. The horizontal grey dash denotes the central estimate for each dataset, while the wider  
215 portion of the bar shows the 66% prediction interval.

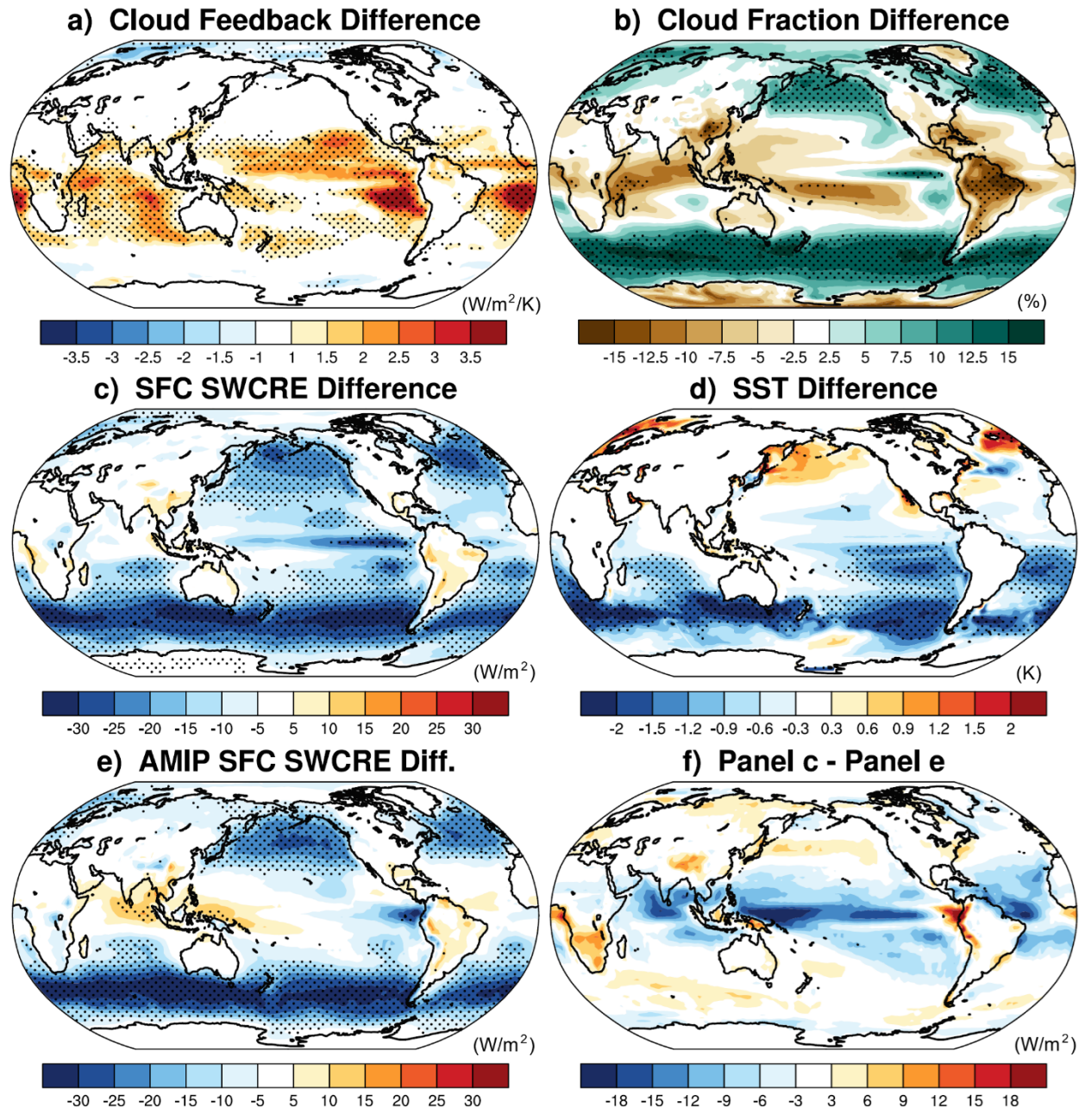
216 The EC yields a TCF value of  $0.52 \pm 0.34 \text{ W/m}^2/\text{K}$ , which represents a 34% reduction in  
217 the likely range of TCF (Fig. 3b). We use a conservative 95% prediction interval (PI) derived  
218 from the hierarchical EC framework (Bowman et al. 2018) to measure the uncertainty reduction  
219 (see Methods). The central estimate of TCF is slightly reduced from the unconstrained ensemble  
220 ( $0.56 \pm 0.51 \text{ W/m}^2/\text{K}$ ). This constraint is also slightly weaker than a prior estimate using monthly  
221 and annual CRE-based tropical cloud variability metrics to constrain TCF (90% confidence  
222 interval of  $-0.22$ - $1.39 \text{ W/m}^2/\text{K}$ ; Lutsko et al. 2021). For reference, we also show the resulting EC  
223 for GCF (Fig. 3d), which exists because of the key role that the tropics play in driving GCF  
224 spread (Fig. S1d-f). This constraint suggests a GCF value of  $0.40 \pm 0.26 \text{ W/m}^2/\text{K}$ , which  
225 represents a 26% reduction in the likely range compared to the unconstrained ensemble ( $0.42 \pm$   
226  $0.35 \text{ W/m}^2/\text{K}$ ). Our constrained GCF estimate also agrees well with the two most notable  
227 community assessments in recent years (Sherwood et al. 2020:  $0.45 \pm 0.33 \text{ W/m}^2/\text{K}$ ; Forster et al.  
228 2021:  $0.42 \pm 0.30 \text{ W/m}^2/\text{K}$ ).

### 229 **3.3 Investigating Drivers of Model Spread**

230 To better understand the relationship between 40–50°S SFC SWCRE and TCF, we group GCMs  
231 by their 40–50°S SFC SWCRE (ten highest and ten lowest across CMIP3/5/6; Tables S1-3) and  
232 assess differences in the subsequent group averages. As per the emergent relationship, the Group  
233 1 models (more negative SFC SWCRE) exhibit much stronger cloud feedback than their Group 2  
234 counterparts (less negative SFC SWCRE) (Fig. 4a). In terms of GCF, their group means are  $0.74$   
235  $\text{W/m}^2/\text{K}$  and  $0.04 \text{ W/m}^2/\text{K}$ , respectively. This discrepancy stems from the tropics, where the

236 difference between group means is even larger ( $1.26 \text{ W/m}^2/\text{K}$ ,  $-0.03 \text{ W/m}^2/\text{K}$ ). This contributes to  
 237 large differences in ECS as well ( $4.35$  vs  $2.85\text{K}$ ). It has been hypothesized that high ECS models  
 238 simulate too many stratocumulus clouds in regions dominated by cumulus clouds, thus producing  
 239 a stronger response of low clouds to warming (Cesena and Del Genio, 2021). However, CMIP  
 240 output does not let us assess these cloud types.

## Group 1 Mean - Group 2 Mean



241  
 242 **Fig. 4.** Maps of the difference in (a) cloud feedback, (b) climatological total cloud fraction, (c) climatological SFC  
 243 SWCRE, and (d) climatological sea surface temperatures between two groups of GCMs defined based on their

244 climatological 40-50°S SFC SWCRE. Group 1 models have a more negative SFC SWCRE than group 2. (e) same as  
245 panel c but derived from AMIP simulations, (f) influence of coupling on the SFC SWCRE difference between the  
246 two groups. Stippling indicates areas of statistical significance determined using a t-test ( $p < 0.05$ ).

247 We find that Group 1 models consistently have greater CLT across extratropical oceans  
248 (Fig. 4b), which is surprising given that Group 2 contains more CMIP6 models (4/10 vs. 3/10),  
249 and that CMIP6 has systematically increased CLT relative to CMIP5 (Fig. S2). Moreover, while  
250 Group 1 models by definition have more negative extratropical SFC SWCRE, this discrepancy  
251 also extends to parts of the tropical oceans (Fig. 4c), particularly where cloud feedback  
252 differences are large (Fig. 4a). Group 1 contains more CMIP3 models, which exhibit  
253 unrealistically bright clouds in the SH subtropics, but similar results hold when CMIP3 is  
254 excluded (Fig. S6). SWCRE differences largely coincide with Group 1 models exhibiting cooler  
255 climatological sea surface temperatures (SSTs) across much of the SH and particularly the  
256 southeast Pacific (Fig. 4d), conditions that favor greater low-level cloud development (Mechoso  
257 et al. 2016). Since similar SFC SWCRE differences are also apparent in AMIP simulations (Fig.  
258 4e), these cooler SSTs are likely driven partly by more negative SFC SWCRE, rather than vice  
259 versa. Fully coupled simulations even enhance SFC SWCRE differences in tropical low-cloud  
260 regions (Fig. 4f). These results agree with past work, which shows that through radiative  
261 perturbation experiments, extratropical energy biases can influence mean-state tropical SSTs and  
262 clouds (Mechoso et al. 2016; Kang et al. 2020; Kang et al. 2023).

### 263 **3.4 Discussion of Mechanisms**

264 The physical mechanisms driving the relationship between climatological SH extratropical SFC  
265 SWCRE and TCF are complex, but we offer some speculation for why this relationship exists. As  
266 suggested above, SH extratropical SWCRE affects tropical low clouds through a teleconnection  
267 likely via the southeast Pacific. Kim et al. (2022) hypothesize that SH extratropical cooling  
268 propagates into the subtropics and is advected further equatorward by climatological winds. This  
269 cooling is then enhanced by a series of processes including the wind-evaporation-SST feedback,

270 stratocumulus cloud feedback, and coastal upwelling. We find that GCMs with more negative 40-  
271 50°S SWCRE tend to exhibit more negative SWCRE and cooler SSTs across tropical low cloud  
272 areas (Fig. 4). These cooler conditions likely help promote greater, more reflective climatological  
273 low clouds in the tropics. In fact, the presence of brighter clouds in Group 1 models becomes  
274 evident across most latitudes when the SWCRE difference between Groups 1 and 2 is  
275 decomposed into contributions from cloud amount and albedo (Fig. S7; see Methods). Therefore,  
276 when these brighter clouds are subjected to future warming, which promotes the loss of low  
277 clouds, the GCM produces a stronger cloud feedback (Fig. 4a). Notably, the Group 1 models also  
278 feature a slightly stronger reduction in tropical CLT (-4.3% compared to -1.3% in Group 2).

279 In contrast to the SH extratropics, mean-state tropical cloud properties are subject to a  
280 variety of influences that mask any relationship with TCF (Fig. 2a-c). For instance, the cloud  
281 brightness differences noted previously are counteracted by greater cloud amount across the  
282 tropics in Group 2 models. This contrasts with the SH, where cloud amount differences enhance  
283 the cloud brightness discrepancy. Moreover, this disconnect between SFC SWCRE and cloud  
284 feedback locally is likely exacerbated by large intermodel differences in tropical cloud coverage  
285 (e.g., in location and extent; Fig. S8) as CLT and SWCRE exhibit their best agreement in low  
286 cloud areas (Fig. S8e). Lastly, the idea that SH extratropical cloud properties are relevant to  
287 tropical clouds is supported by a moderate correlation between 40-50°S SWCRE in CMIP5-6  
288 with two climatological cloud metrics computed across the tropics (deseasonalized monthly and  
289 annual CRE sensitivities) from Lutsko et al. (2021) (Fig. S9).

#### 290 **4. Conclusions**

291 Using climatological biases for ECs is a potentially promising avenue for research as it gives  
292 modeling centers a relatively easy target metric to monitor during development stages. Here, we  
293 use three ensembles of GCMs to explore the potential of using climatological biases in clouds for  
294 constraining regional cloud feedback. We find the greatest value in climatological SFC SWCRE

295 across the SH mid-latitudes (40-50°S), which is strongly tied ( $|r| \geq 0.7$ ) to TCF in all generations.  
296 Using this relationship in conjunction with observations, we produce an EC on TCF, which  
297 suggests a TCF of  $0.52 \pm 0.34$  W/m<sup>2</sup>/K, compared to the unconstrained estimate of  $0.56 \pm 0.51$   
298 W/m<sup>2</sup>/K. This suggests that the model mean is slightly too strong, while also representing a 34%  
299 reduction in model uncertainty. Given the importance of the tropics to GCF, 40-50°S SFC  
300 SWCRE can also be used to infer a GCF value of  $0.40 \pm 0.26$  W/m<sup>2</sup>/K, which agrees well with  
301 two notable community assessments (Sherwood et al. 2020; Forster et al. 2021).

302 Past research identified various metrics as potentially relevant to variability in TCF/GCF.  
303 This includes parametric differences in extratropical mixed phase cloud partitioning (McCoy et al.  
304 2016). While we find this metric (known as T5050: temperature where ice and liquid phases are  
305 equal) to be only weakly correlated with 40-50°S SFC SWCRE across a set of 23 CMIP5/6  
306 models ( $r = -0.16$ ), it is possible that there are other unknown GCM tuning dynamics at play here.  
307 Our results also suggest that the warm-cold SWCRE gradient is not useful beyond CMIP5,  
308 potentially at odds with prior work (see Text S3). As past studies have noted, finding these  
309 relationships is the first step to understanding them, but healthy skepticism should be maintained  
310 about this EC until it is better understood (Caldwell et al. 2014; Klein and Hall, 2015). Future  
311 work should seek to better understand mechanisms and the sources of model bias in SFC SWCRE  
312 across the SH extratropics.

313



## 314 **Acknowledgements**

315 We acknowledge funding from the Regional and Global Model Analysis Program for the Office  
316 of Science of the U.S. Department of Energy through the Program for Climate Model Diagnosis  
317 and Intercomparison (PCMDI). The work of M. D. Zelinka and S. Po-Chedley was performed  
318 under the auspices of the U.S. Department of Energy by Lawrence Livermore National  
319 Laboratory under contract DE-AC52-07NA27344. We thank the World Climate Research  
320 Programme's Working Group on Coupled Modeling and the individual modeling groups for their  
321 roles in making CMIP data available. We also thank the two reviewers for their constructive  
322 feedback.

## 324 **Open Research**

325 All data used in this study is publicly available. The CMIP output (models listed in Tables S1-S3)  
326 is available from the Earth System Grid Federation (<https://aims2.llnl.gov/search>). CERES data is  
327 available from: <https://ceres.larc.nasa.gov/data/>. Data from ERA5 (Hersbach et al. 2023) were  
328 also used in the creation of this manuscript. The code relating to this study (Thackeray et al. 2024)  
329 is available from: <https://github.com/cwthackeray/GRL-clouds>.

330 **References**

- 331 Bony, S., & Dufresne, J. L. (2005). Marine boundary layer clouds at the heart of tropical cloud  
332 feedback uncertainties in climate models. *Geophysical Research Letters*, 32(20), 1–4.  
333 <https://doi.org/10.1029/2005GL023851>
- 334 Bony, S., Colman, R., Kattsov, V. M., Allan, R. P., Bretherton, C. S., Dufresne, J. L., Hall, A.,  
335 Hallegatte, S., Holland, M. M., Ingram, W., Randall, D. A., Soden, B. J., Tselioudis, G., & Webb,  
336 M. J. (2006). How well do we understand and evaluate climate change feedback processes?  
337 *Journal of Climate*, 19, 3445–3482. <https://doi.org/10.1175/JCLI3819.1>
- 338 Bowman, K. W., Cressie, N., Qu, X., & Hall, A. (2018). A Hierarchical Statistical Framework for  
339 Emergent Constraints: Application to Snow-Albedo Feedback. *Geophysical Research Letters*,  
340 45(23), 13,050–13,059. <https://doi.org/10.1029/2018GL080082>
- 341 Brient, F., & Schneider, T. (2016). Constraints on climate sensitivity from space-based  
342 measurements of low-cloud reflection. *Journal of Climate*, 29(16), 5821–5835.  
343 <https://doi.org/10.1175/JCLI-D-15-0897.1>
- 344 Brient, F., Schneider, T., Tan, Z., Bony, S., Qu, X., & Hall, A. (2016). Shallowness of tropical  
345 low clouds as a predictor of climate models' response to warming. *Climate Dynamics*, 47(1–2),  
346 433–449. <https://doi.org/10.1007/s00382-015-2846-0>
- 347 Caldwell, P. M., Bretherton, C. S., Zelinka, M. D., Klein, S. A., Santer, B. D., & Sanderson, B.  
348 M. (2014). Statistical significance of climate sensitivity predictors obtained by data mining.  
349 *Geophysical Research Letters*, 41(5), 1803–1808. <https://doi.org/10.1002/2014GL059205>
- 350 Caldwell, P. M., Zelinka, M. D., & Klein, S. A. (2018). Evaluating emergent constraints on  
351 equilibrium climate sensitivity. *Journal of Climate*, 31(10), 3921–3942.  
352 <https://doi.org/10.1175/JCLI-D-17-0631.1>
- 353 Caldwell, P. M., Zelinka, M. D., Taylor, K. E., & Marvel, K. (2016). Quantifying the sources of  
354 intermodel spread in equilibrium climate sensitivity. *Journal of Climate*, 29(2), 513–524.  
355 <https://doi.org/10.1175/JCLI-D-15-0352.1>
- 356 Cesana, G. v., & del Genio, A. D. (2021). Observational constraint on cloud feedbacks suggests  
357 moderate climate sensitivity. *Nature Climate Change*, 11(3), 213–218.  
358 <https://doi.org/10.1038/s41558-020-00970-y>
- 359 Cess, R. D., Potter, G. L., Blanchet, J. P., Boer, G. J., Genio, A. D. D., D'É Qu'É, M., Dymnikov,  
360 V., Galin, V., Gates, W. L., Ghan, S. J., Kiehl, J. T., Lacis, A. A., Treut, H. le, Li, Z. X., Liang, X.  
361 Z., McAvaney, B. J., Meleshko, V. P., Mitchell, J. F. B., Morcrette, J. J., ... Zhang, M. H.  
362 (1990). Intercomparison and interpretation of climate feedback processes in 19 atmospheric

363 general circulation models. *Journal of Geophysical Research*, 95(D10).  
364 <https://doi.org/10.1029/jd095id10p16601>

365 Eyring, V., Bony, S., Meehl, G. A., Senior, C. A., Stevens, B., Stouffer, R. J., & Taylor, K. E.  
366 (2016). Overview of the Coupled Model Intercomparison Project Phase 6 (CMIP6) experimental  
367 design and organization. *Geoscientific Model Development*, 9(5), 1937–1958.  
368 <https://doi.org/10.5194/gmd-9-1937-2016>

369 Forster, P., T. Storelvmo, K. Armour, W. Collins, J.-L. Dufresne, D. Frame, D.J. Lunt, T.  
370 Mauritsen, M.D. Palmer, M. Watanabe, M. Wild, and H. Zhang, The Earth’s Energy Budget,  
371 Climate Feedbacks, and Climate Sensitivity. In *Climate Change 2021: The Physical Science*  
372 *Basis. Contribution of Working Group I to the Sixth Assessment Report of the Intergovernmental*  
373 *Panel on Climate Change* [Masson-Delmotte, V., P. Zhai, A. Pirani, S.L. Connors, C. Péan, S.  
374 Berger, N. Caud, Y. Chen, L. Goldfarb, M.I. Gomis, M. Huang, K. Leitzell, E. Lonnoy, J.B.R.  
375 Matthews, T.K. Maycock, T. Waterfield, O. Yelekçi, R. Yu, and B. Zhou (eds.)]. Cambridge  
376 University Press, Cambridge, United Kingdom and New York, NY, USA, 923–1054 (2021).

377 Gettelman, A., Hannay, C., Bacmeister, J. T., Neale, R. B., Pendergrass, A. G., Danabasoglu, G.,  
378 Lamarque, J. -F., Fasullo, J. T., Bailey, D. A., Lawrence, D. M., & Mills, M. J. (2019). High  
379 Climate Sensitivity in the Community Earth System Model Version 2 (CESM2). *Geophysical*  
380 *Research Letters*, 46(14), 8329–8337. <https://doi.org/10.1029/2019gl083978>

381 Grise, K. M., Polvani, L. M., & Fasullo, J. T. (2015). Reexamining the relationship between  
382 climate sensitivity and the Southern Hemisphere radiation budget in CMIP models. *Journal of*  
383 *Climate*, 28(23), 9298–9312. <https://doi.org/10.1175/JCLI-D-15-0031.1>

384 Hall, A., Cox, P., Huntingford, C., & Klein, S. (2019). Progressing emergent constraints on future  
385 climate change. *Nature Climate Change*, 9(4), 269–278. [https://doi.org/10.1038/s41558-019-](https://doi.org/10.1038/s41558-019-0436-6)  
386 [0436-6](https://doi.org/10.1038/s41558-019-0436-6)

387 Hersbach, H., Bell, B., Berrisford, P., Biavati, G., Horányi, A., Muñoz Sabater, J., Nicolas, J.,  
388 Peubey, C., Radu, R., Rozum, I., Schepers, D., Simmons, A., Soci, C., Dee, D., Thépaut, J.-N.  
389 (2023). ERA5 monthly averaged data on single levels from 1940 to present. Copernicus Climate  
390 Change Service (C3S) Climate Data Store (CDS) [Dataset].  
391 <https://doi.org/10.24381/cds.f17050d7>

392 Hersbach, H., Bell, B., Berrisford, P., Hirahara, S., Horányi, A., Muñoz-Sabater, J., Nicolas, J.,  
393 Peubey, C., Radu, R., Schepers, D., Simmons, A., Soci, C., Abdalla, S., Abellan, X., Balsamo, G.,  
394 Bechtold, P., Biavati, G., Bidlot, J., Bonavita, M., ... Thépaut, J. N. (2020). The ERA5 global  
395 reanalysis. *Quarterly Journal of the Royal Meteorological Society*, 146(730), 1999–2049.  
396 <https://doi.org/10.1002/qj.3803>

397 Hirota, N., Ogura, T., Shiogama, H., Caldwell, P., Watanabe, M., Kamae, Y., & Suzuki, K.  
398 (2021). Underestimated marine stratocumulus cloud feedback associated with overly active deep  
399 convection in models. *Environmental Research Letters*, 16(7). [https://doi.org/10.1088/1748-](https://doi.org/10.1088/1748-9326/abfb9e)  
400 9326/abfb9e

401 Jiang, X., Su, H., Jiang, J. H., Neelin, J. D., Wu, L., Tsushima, Y., & Elsaesser, G. (2023). Muted  
402 extratropical low cloud seasonal cycle is closely linked to underestimated climate sensitivity in  
403 models. *Nature Communications*, 14(5586). <https://doi.org/10.1038/s41467-023-41360-0>

404 Kang, S. M., Ceppi, P., Yu, Y., & Kang, I. S. (2023). Recent global climate feedback controlled  
405 by Southern Ocean cooling. *Nature Geoscience*, 16(9), 775–780. [https://doi.org/10.1038/s41561-](https://doi.org/10.1038/s41561-023-01256-6)  
406 023-01256-6

407 Kang, S. M., Hawcroft, M., Xiang, B., Hwang, Y. T., Cazes, G., Codron, F., Crueger, T., Deser,  
408 C., Hodnebrog, Ø., Kim, H., Kim, J., Kosaka, Y., Losada, T., Mechoso, C. R., Myhre, G., Seland,  
409 Ø., Stevens, B., Watanabe, M., & Yu, S. (2019). Extratropical–tropical interaction model  
410 intercomparison project (ETIN-MIP): Protocol and initial results. *Bulletin of the American*  
411 *Meteorological Society*, 100(12), 2589–2605. <https://doi.org/10.1175/BAMS-D-18-0301.1>

412 Kang, S. M., Xie, S.-P., Shin, Y., Kim, H., Hwang, Y.-T., Stuecker, M. F., Xiang, B., &  
413 Hawcroft, M. (2020). Walker circulation response to extratropical radiative forcing. *Science*  
414 *Advances*, 6.

415 Kato, S., Rose, F. G., Rutan, D. A., Thorsen, T. J., Loeb, N. G., Doelling, D. R., Huang, X.,  
416 Smith, W. L., Su, W., & Ham, S. H. (2018). Surface irradiances of edition 4.0 Clouds and the  
417 Earth’s Radiant Energy System (CERES) Energy Balanced and Filled (EBAF) data product.  
418 *Journal of Climate*, 31(11), 4501–4527. <https://doi.org/10.1175/JCLI-D-17-0523.1>

419 Kay, J. E., Bourdages, L., Miller, N. B., Morrison, A., Yettella, V., Chepfer, H., & Eaton, B.  
420 (2016). Evaluating and improving cloud phase in the Community Atmosphere Model version 5  
421 using spaceborne lidar observations. *Journal of Geophysical Research: Atmospheres*, 1–19.  
422 <https://doi.org/10.1002/2014JD022994>.Received

423 Klein, S. A., & Hall, A. (2015). Emergent Constraints for Cloud Feedbacks. *Current Climate*  
424 *Change Reports*, 1(4), 276–287. <https://doi.org/10.1007/s40641-015-0027-1>

425 Klein, S. A., Zhang, Y., Zelinka, M. D., Pincus, R., Boyle, J., & Gleckler, P. J. (2013). Are  
426 climate model simulations of clouds improving? An evaluation using the ISCCP simulator.  
427 *Journal of Geophysical Research Atmospheres*, 118(3), 1329–1342.  
428 <https://doi.org/10.1002/jgrd.50141>

429 Lauer, A., Bock, L., Hassler, B., Schröder, M., & Stengel, M. (2023). Cloud Climatologies from  
430 Global Climate Models-A Comparison of CMIP5 and CMIP6 Models with Satellite Data. *Journal*  
431 *of Climate*, 36(2), 281–311. <https://doi.org/10.1175/JCLI-D-22-0181.1>

432 Lauer, A., & Hamilton, K. (2013). Simulating clouds with global climate models: A comparison  
433 of CMIP5 results with CMIP3 and satellite data. *Journal of Climate*, 26(11), 3823–3845.  
434 <https://doi.org/10.1175/JCLI-D-12-00451.1>

435 Lipat, B. R., Tselioudis, G., Grise, K. M., & Polvani, L. M. (2017). CMIP5 models' shortwave  
436 cloud radiative response and climate sensitivity linked to the climatological Hadley cell extent.  
437 *Geophysical Research Letters*, 44(11), 5739–5748. <https://doi.org/10.1002/2017GL073151>

438 Loeb, N. G., Doelling, D. R., Wang, H., Su, W., Nguyen, C., Corbett, J. G., Liang, L., Mitrescu,  
439 C., Rose, F. G., & Kato, S. (2018). Clouds and the Earth's Radiant Energy System (CERES)  
440 Energy Balanced and Filled (EBAF) top-of-atmosphere (TOA) edition-4.0 data product. *Journal*  
441 *of Climate*, 31(2), 895–918. <https://doi.org/10.1175/JCLI-D-17-0208.1>

442 Lutsko, N. J., Popp, M., Nazarian, R. H., & Albright, A. L. (2021). Emergent Constraints on  
443 Regional Cloud Feedbacks. *Geophysical Research Letters*, 48(10).  
444 <https://doi.org/10.1029/2021GL092934>

445 McCoy, D. T., Field, P., Bodas-Salcedo, A., Elsaesser, G. S., & Zelinka, M. D. (2020). A  
446 Regime-Oriented Approach to Observationally Constraining Extratropical Shortwave Cloud  
447 Feedbacks. *Journal of Climate*, 33(23), 9967–9983. <https://doi.org/10.1175/jcli-d-19-0987.1>

448 McCoy, D. T., Tan, I., Hartmann, D. L., Zelinka, M. D., & Storelvmo, T. (2016). On the  
449 relationships among cloud cover, mixed-phase partitioning, and planetary albedo in GCMs.  
450 *Journal of Advances in Modeling Earth Systems*, 8(2), 650–668.  
451 <https://doi.org/10.1002/2015MS000589>

452 Mechoso, C. R., Losada, T., Koseki, S., Mohino-Harris, E., Keenlyside, N., Castaño-Tierno, A.,  
453 Myers, T. A., Rodriguez-Fonseca, B., & Toniazzo, T. (2016). Can reducing the incoming energy  
454 flux over the Southern Ocean in a CGCM improve its simulation of tropical climate? *Geophysical*  
455 *Research Letters*, 43(20), 11,057–11,063. <https://doi.org/10.1002/2016GL071150>

456 Meehl, G. A., Covey, C., Delworth, T., Latif, M., McAvaney, B., Mitchell, J. F. B., Stouffer, R.  
457 J., & Taylor, K. E. (2007). The WCRP CMIP3 multimodel dataset: A new era in climatic change  
458 research. *Bulletin of the American Meteorological Society*, 88(9), 1383–1394.  
459 <https://doi.org/10.1175/BAMS-88-9-1383>

460 Myers, T. A., & Norris, J. R. (2016). Reducing the uncertainty in subtropical cloud feedback.  
461 *Geophysical Research Letters*, 43(5), 2144–2148. <https://doi.org/10.1002/2015GL067416>

462 Myers, T. A., Scott, R. C., Zelinka, M. D., Klein, S. A., Norris, J. R., & Caldwell, P. M. (2021).  
463 Observational constraints on low cloud feedback reduce uncertainty of climate sensitivity. *Nature*  
464 *Climate Change*, 11(6), 501–507. <https://doi.org/10.1038/s41558-021-01039-0>

465 Nam, C., Bony, S., Dufresne, J. L., & Chepfer, H. (2012). The too few, too bright tropical low-  
466 cloud problem in CMIP5 models. *Geophysical Research Letters*, 39(21).  
467 <https://doi.org/10.1029/2012GL053421>

468 Qu, X., Hall, A., Klein, S. A., & Caldwell, P. M. (2014). On the spread of changes in marine low  
469 cloud cover in climate model simulations of the 21st century. *Climate Dynamics*, 42(9–10), 2603–  
470 2626. <https://doi.org/10.1007/s00382-013-1945-z>

471 Qu, X., Hall, A., Klein, S. A., & Deangelis, A. M. (2015). Positive tropical marine low-cloud  
472 cover feedback inferred from cloud-controlling factors. *Geophysical Research Letters*, 42(18),  
473 7767–7775. <https://doi.org/10.1002/2015GL065627>

474 Schlund, M., Lauer, A., Gentine, P., Sherwood, S. C., & Eyring, V. (2020). Emergent constraints  
475 on equilibrium climate sensitivity in CMIP5: Do they hold for CMIP6? *Earth System Dynamics*,  
476 11(4), 1233–1258. <https://doi.org/10.5194/esd-11-1233-2020>

477 Shell, K. M., Kiehl, J. T., & Shields, C. a. (2008). Using the radiative kernel technique to  
478 calculate climate feedbacks in NCAR’s Community Atmospheric Model. *Journal of Climate*, 21,  
479 2269–2282. <https://doi.org/10.1175/2007JCLI2044.1>

480 Sherwood, S., Webb, M. J., Annan, J. D., Armour, K. C., Forster, P. M., Hargreaves, J. C.,  
481 Hegerl, G., Klein, S. A., Marvel, K. D., Rohling, E. J., Watanabe, M., Andrews, T., Braconnot, P.,  
482 Bretherton, C. S., Foster, G. L., Hausfather, Z., Heydt, A. S. von der, Knutti, R., Mauritsen, T., ...  
483 Zelinka, M. D. (2020). An assessment of Earth’s climate sensitivity using multiple lines of  
484 evidence. *Reviews of Geophysics*, 58, e2019RG000678. <https://doi.org/10.1029/2019RG000678>

485 Siler, N., Po-Chedley, S., & Bretherton, C. S. (2018). Variability in modeled cloud feedback tied  
486 to differences in the climatological spatial pattern of clouds. *Climate Dynamics*, 50(3–4), 1209–  
487 1220. <https://doi.org/10.1007/s00382-017-3673-2>

488 Soden, B. J., Held, I. M., Colman, R. C., Shell, K. M., Kiehl, J. T., & Shields, C. a. (2008).  
489 Quantifying climate feedbacks using radiative kernels. *Journal of Climate*, 21(1988), 3504–3520.  
490 <https://doi.org/10.1175/2007JCLI2110.1>

491 Taylor, K. E., Stouffer, R. J., & Meehl, G. A. (2012). An Overview of CMIP5 and the Experiment  
492 Design. *Bulletin of the American Meteorological Society*, 3(April), 485–498.  
493 <https://doi.org/10.1175/BAMS-D-11-00094.1>

494 Terai, C. R., Klein, S. A., & Zelinka, M. D. (2016). Constraining the low-cloud optical depth  
495 feedback at middle and high latitudes using satellite observations. *Journal of Geophysical*  
496 *Research*, 121(16), 9696–9716. <https://doi.org/10.1002/2016JD025233>

497 Thackeray, C. W. (2024). cwthackeray/GRL-clouds: Thackeray24 (Version 1.0.0) [Software].  
498 Zenodo. <https://doi.org/10.5281/zenodo.14226936>

499 Tian, B. (2015). Spread of model climate sensitivity linked to double-Intertropical Convergence  
500 Zone bias. *Geophysical Research Letters*, 42(10), 4133–4141.  
501 <https://doi.org/10.1002/2015GL064119>

502 Trenberth, K. E., & Fasullo, J. T. (2010). Simulation of present-day and twenty-first-century  
503 energy budgets of the southern oceans. *Journal of Climate*, 23(2), 440–454.  
504 <https://doi.org/10.1175/2009JCLI3152.1>

505 Vignesh, P. P., Jiang, J. H., Kishore, P., Su, H., Smay, T., Brighton, N., & Velicogna, I. (2020).  
506 Assessment of CMIP6 Cloud Fraction and Comparison with Satellite Observations. *Earth and*  
507 *Space Science*, 7(2). <https://doi.org/10.1029/2019EA000975>

508 Volodin, E. M. (2008). Relation between temperature sensitivity to doubled carbon dioxide and  
509 the distribution of clouds in current climate models. *Izvestiya, Atmospheric and Oceanic Physics*,  
510 44(3), 288–299. <https://doi.org/10.1134/S0001433808030043>

511 Wall, C. J., Storelvmo, T., Norris, J. R., & Tan, I. (2022). Observational Constraints on Southern  
512 Ocean Cloud-Phase Feedback. *Journal of Climate*, 35, 5087–5102. [https://doi.org/10.1175/JCLI-](https://doi.org/10.1175/JCLI-D-21)  
513 [D-21](https://doi.org/10.1175/JCLI-D-21)

514 Webb, M. J., Lambert, F. H., & Gregory, J. M. (2013). Origins of differences in climate  
515 sensitivity, forcing and feedback in climate models. *Climate Dynamics*, 40(3–4), 677–707.  
516 <https://doi.org/10.1007/s00382-012-1336-x>

517 Webb, M. J., & Lock, A. P. (2020). Testing a Physical Hypothesis for the Relationship Between  
518 Climate Sensitivity and Double-ITCZ Bias in Climate Models. *Journal of Advances in Modeling*  
519 *Earth Systems*, 12. <https://doi.org/10.1029/2019MS001999>

520 Williams, K. D., & Tselioudis, G. (2007). GCM intercomparison of global cloud regimes:  
521 Present-day evaluation and climate change response. *Climate Dynamics*, 29(2–3), 231–250.  
522 <https://doi.org/10.1007/s00382-007-0232-2>

523 Williamson, M. S., Thackeray, C. W., Cox, P. M., Hall, A., Huntingford, C., & Nijssen, F. J. M. M.  
524 (2021). Emergent constraints on climate sensitivities. *Reviews of Modern Physics*, 93(2), 025004.  
525 <https://doi.org/10.1103/RevModPhys.93.025004>

526 Zelinka, M. D., Myers, T. A., McCoy, D. T., Po-Chedley, S., Caldwell, P. M., Ceppi, P., Klein, S.  
527 A., & Taylor, K. E. (2020). Causes of Higher Climate Sensitivity in CMIP6 Models. *Geophysical*  
528 *Research Letters*, 47(1), e2019GL085782. <https://doi.org/10.1029/2019GL085782>

529 Zhai, C., Jiang, J. H., & Su, H. (2015). Long-term cloud change imprinted in seasonal cloud  
530 variation: More evidence of high climate sensitivity. *Geophysical Research Letters*, 42(20),  
531 8729–8737. <https://doi.org/10.1002/2015GL065911>

532 Zhou, C., Zelinka, M. D., Dessler, A. E., & Klein, S. A. (2015). The relationship between  
533 interannual and long-term cloud feedbacks. *Geophysical Research Letters*, 42(23), 10463–10469.  
534 <https://doi.org/10.1002/2015GL066698>

535 Zhou, W., Leung, L. R., Siler, N., & Lu, J. (2023). Future precipitation increase constrained by  
536 climatological pattern of cloud effect. *Nature Communications*, 14(1), 6363.  
537 <https://doi.org/10.1038/s41467-023-42181-x>

538 Zhu, J., Otto-Bliesner, B. L., Brady, E. C., Gettelman, A., Bacmeister, J. T., Neale, R. B.,  
539 Poulsen, C. J., Shaw, J. K., McGraw, Z. S., & Kay, J. E. (2022). LGM Paleoclimate Constraints  
540 Inform Cloud Parameterizations and Equilibrium Climate Sensitivity in CESM2. *Journal of*  
541 *Advances in Modeling Earth Systems*, 14(4). <https://doi.org/10.1029/2021MS002776>

542